We are IntechOpen,
the world's leading publisher of
Open Access books
Built by scientists, for scientists

6,900
Open access books available

186,000
International authors and editors

200M
Downloads

Our authors are among the

154
Countries delivered to

TOP 1%
most cited scientists

12.2%
Contributors from top 500 universities

CLARIVATE ANALYTICS
BOOK CITATION INDEX
INDEXED

WEB OF SCIENCE™

Selection of our books indexed in the Book Citation Index
in Web of Science™ Core Collection (BKCI)

Interested in publishing with us?
Contact book.department@intechopen.com

Numbers displayed above are based on latest data collected.
For more information visit www.intechopen.com

Chapter

Designing and Synthesis of (Cd^{2+}, Li^+), Cr^{3+}, Bi^{3+} Doped $CePO_4$ Materials Optical, Electrochemical, Ionic Conductivity Analysis

Salah Kouass, Amor Fadhalaoui, Hassouna Dhaouadi and Fathi Touati

Abstract

Most of the work has been done on the optical properties of the rare earth doped $CePO_4$, so there are few studies on the effect of metal ion doping on $CePO_4$. The doping improves the properties of the compounds and can lead to new properties. **It is the first time, that multi- ionic doping process is used in the $CePO_4$ matrix, in order to improve the ionic conductivity and the electrochemical stability.** The low percentage of (Cd^{2+}, Li^+), Cr^{3+}, Bi^{3+} dopant affect the structure showing a weak decrease in the lattice parameters compared to the $CePO_4$. Impedance spectroscopy analysis was used to analyze the electrical behavior of samples as a function of frequency at different temperatures. The total electrical conductivity plots obtained from impedance spectra shows an increase of the total conductivity as Li, Cr-content increases. The determined energy gap values decrease with increasingly Li^+, Cr^{3+} and Bi^{3+} doping content. Electrochemical tests showed an improved capacity when increasing the Li^+, Cr^{3+} and Bi^{3+} content and a stable cycling performance.

Keywords: phosphate materials, doping, optical properties, impedance spectroscopy, electrochemical properties

1. Introduction

Nanoscience and nanotechnology is a rapid-developing field which has demanded the technologist to innovate applicable nanomaterials with manipulated shape and size to explore their principal chemical and physical characteristics [1]. In recent years, rare earth phosphates have attracted many researchers because of their technological applications [2, 3]. Cerium orthophosphate **nanomaterials** have important properties: high thermal stability [4], **very low solubility in water, their use in the production of moisture sensors for luminescent materials, a poison for automotive catalysts and a novel oxygen sensing material on the basis of its redox responsive reversible luminescence** [5–7].

Most of the work has been done on the optical properties of the rare earth doped CePO$_4$, so there are few studies on the effect of metal ion doping on CePO$_4$. Additionally, CePO$_4$ materials have been used in hydrogen fuel cells [8]. To better understand the mechanism of conduction, information on the behavior and ionic conductivities of charge carriers located in phosphates, electrical studies have been carried out.

Generally, the doping process improves the properties of the compounds and can lead to new properties [9, 10]. Trivalent elements have been known as doping elements, improving the physico-chemical properties of cerium phosphate-based materials [11]. In order to improve the electrical and optical properties, the cerium phosphate was partially substituted by divalent transition metal ions. The doping with Ca and Sr. has improved the electrical conductivity of (La, Ce) PO$_4$ [12, 13]. The high conductivity of the Sr-doped CePO$_4$ under wet oxidizing conditions due to electronic and ionic conduction is shown by Moral et al. [12]. Norby et al. studied the effect of the substitution of lanthanum by calcium and strontium on the conductivity, described by the dependence on humidity and the effect of H/D isotopic exchange [13].

The substitution effect depends on the nature of the doping elements. Chromium shows the stability of the valence state (+ III) in conductive p-type SOFC interconnection materials [14]. Numerous reports show that substitution with Cr^{3+} ions introduces interesting properties in ferrites [15, 16]. Cr-doping CePO$_4$ is expected to improve its optical and electrical properties.

Bismuth-based materials have been studied because of their excellent photocatalytic activities in the reduction of NO [17], the generation of O$_2$ [18, 19] and the decomposition of organic compounds [20, 21]. **It was founded that Y$_2$SiO$_5$:Bi^{3+} gives rise to three emission bands centering at: 355, 408, and 504 nm upon UV excitation possibly from three types of bismuth emission centers in the compound, respectively [22]. The broad absorption band of Bi^{3+} improves the emission process which could be varied from the UV to the NIR, depending on its final valence in the compounds** [23]. The Bi^{3+} ions combined with rare earth ions such as cerium, Ce^{3+}, can improve the optical properties of CePO$_4$ nanomaterials. The study of the effect of doping with Bi^{3+} ions on the structural and electrical properties of CePO$_4$ is virgin. This leads to new optical and electrical properties for application in electronic devices.

Divalent cations were doped in monophosphates, giving variations in the electrical properties of these doped materials. The aim is to study the combined effect of monovalent Li$^+$ and divalent Cd^{2+} ions on structural, electrical and optical properties. Indeed, the electrical and electrochemical properties of cadmium allow it to be used in mobile phone batteries [24, 25]. Also lithium Li$^+$ ions associated with the divalent Fe^{2+}, Mn^{2+} and Co^{2+} ions favor the increase of the capacity, the lifetime, **diffusion process** and the electrochemical stability of a phosphate-based electrode [26–28]. **The adjustment of the size, shape, density, optical, electrical and dielectric properties of nanoparticles could help tune their broad spectral resonance wavelength [29]. Microemulsion approach associated to the hydrothermal conditions could be used to fabricate single crystalline CePO$_4$ nanowires with controlled aspect ratios [30]. Hydrothermal process has emerged as a powerful tool due to some significant advantages such as cost-effective, controllable particle size, low-temperature and less-complicated techniques [31].**

2. Characterizations

Cerium orthophosphate has two crystalline phases [32, 33]. At low temperature this material crystallizes in the hexagonal system. At high temperature cerium

orthophosphate crystallizes in the monoclinic system. The hexagonal structure is characterized by the existence of large tunnels parallel to the c-axis in which the water present in the compound appears to be localized. The $CePO_4$ produced in aqueous solution at room temperature crystallizes in a hexagonal form [34, 35]. After heat treatment at 650°C, the hexagonal phase ($CePO_4$) started converting into a monoclinic structure.

The ions (Cd^{2+}, Li^+), Cr^{3+}, Bi^{3+} doped $CePO_4$ materials were characterized by X-ray diffraction (XRD). All samples are single phase having a hexagonal structure similar to $CePO_4$. **The** 2θ values of doped materials shift slightly higher angles with increasing Cr, Bi, Cd and Li content, confirming the complete dissolution of dopants (**Figure 1**). The same behavior was observed when Fe^{3+} ion substitutes La^{3+} ion in $LaPO_4$ [36]. The average crystallite size of all samples decreases with increasing the amount of doping. The main reason for the decrease of the grain size may be due to the fact that doping introduced defects and the defects prevent grain to grow [37].

Many parameters affecting the morphological characteristics of the hexagonal cerium phosphate nanocrystals such as the cerium concentration, the treatment temperature, the reaction time, the nature of the surfactant, the pH value of the solution and the synthesis method. The materials take on a similar shape to the nanorod morphology with the size depending on the dopant-content.

3. Optical properties

The band gap energy of the as-prepared samples was calculated using the Kubelka-Munk plot. The Kubelka-Munk function for diffuse reflectance [38] is

$$f(R) = \frac{1 - R^2}{2.R} \tag{1}$$

where R is the reflectance. The optical band gap, E_g, can be determined using the Tauc relation:

$$[F(R).h\nu] = A[h\nu - E_g]^n \tag{2}$$

where A is an energy-independent constant, E_g is the optical band gap and n can take values of 0.5, 1.5, 2 and 3 depending on the mode of transition [39]. The band gap energies can be estimated by extrapolating the linear portions to the $h\nu$ axis and from the corresponding intercept of the tangents to the plots of $[F(R)^*h\nu]^2$ vs. $h\nu$.

The determined energy gap values decrease with increasing Cr, Bi, Cd and Li-doping content in $Cr_xCe_{1-x}PO_4$ (x = 0.00, 0.08, 0.10 and 0.20), $Bi_xCe_{1-x}PO_4$ (x = 0.00, 0.02 and 0.08), $Ce_{0.9}Cd_{0.15-x}Li_{2x}PO_4$ (x = 0 and 0.02) nanorods,
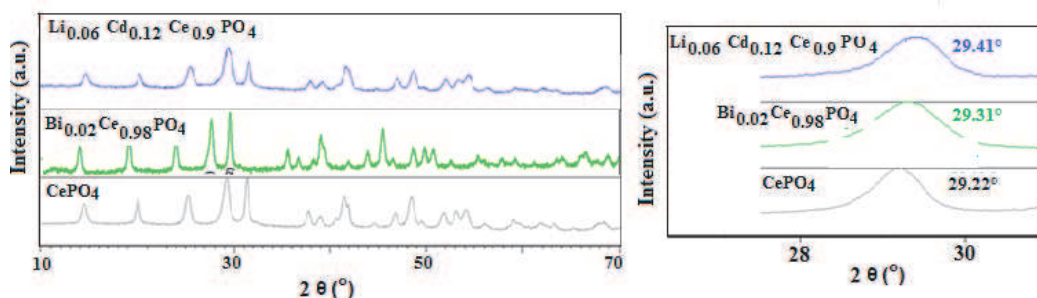
Figure 1.
X-ray diffraction pattern of $CePO_4$, $Bi_{0.02}Ce_{0.98}PO_4$ and $Li_{0.06}Cd_{0.12}Ce_{0.90}PO_4$.
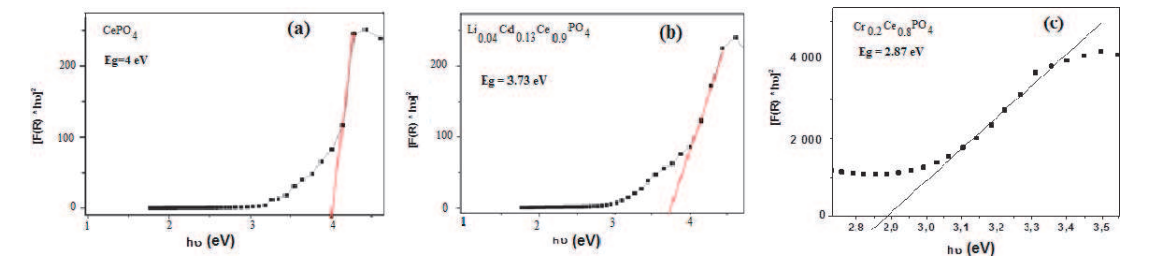
Figure 2.
[f(R) × hυ]2 versus the hυ (eV) plots of: (a) CePO$_4$; (b): Ce$_{0.9}$Cd$_{0.13}$Li$_{0.04}$PO$_4$; and (c) Cr$_{0.20}$Ce$_{0.80}$PO$_4$.

Cr$_x$Ce$_{1-x}$PO$_4$ Eg (eV) [40]	Bi$_x$Ce$_{1-x}$PO$_4$ Eg (eV) [41]	Ce$_{0.9}$Cd$_{0.15-x}$Li$_{2x}$PO$_4$ Eg (eV) [42]
CePO$_4$ Eg = 4.14	CePO$_4$ Eg = 4.00	CePO$_4$ Eg = 4.00
Cr$_{0.08}$Ce$_{0.92}$PO$_4$ Eg = 4.10	Bi$_{0.02}$Ce$_{0.98}$PO$_4$ Eg = 3.96	Ce$_{0.9}$Cd$_{0.15}$PO$_4$ Eg = 3.95
Cr$_{0.10}$Ce$_{0.90}$PO$_4$ Eg = 3.09	Bi$_{0.08}$Ce$_{0.92}$PO$_4$ Eg = 3.84	Ce$_{0.9}$Cd$_{0.13}$Li$_{0.04}$PO$_4$ Eg = 3.73
Cr$_{0.20}$Ce$_{0.80}$PO$_4$ Eg = 2.87		

Table 1.
Gap energy values of Cr$_x$Ce$_{1-x}$PO$_4$, Bi$_x$Ce$_{1-x}$PO$_4$ and Ce$_{0.9}$Cd$_{0.15-x}$Li$_{2x}$PO$_4$ nanomaterials.

respectively, showing a red-shift trend when the doping- substitution percentage increases (**Figure 2**). **Table 1** summarizes the gap energy values of nanomaterials.

The size, morphology and substitution of crystallites affect the energy of the band gap. The substitution of Ce^{3+} by a transition metal could induce the formation of several structural defects, creating different energy levels below the conduction band. The same behavior has been observed in Cr-doped Ni$_3$(PO$_4$)$_2$ where the band gap decreases when Cr^{3+} replaces Ni^{2+} [43].

4. Electrical conductivity

The dc-conductivity (σ_{dc}) of Bi$_x$Ce$_{1-x}$PO$_4$ could be calculated using the Formula's

$$\sigma_{dc} = \frac{t}{A} * \frac{1}{R} \tag{3}$$
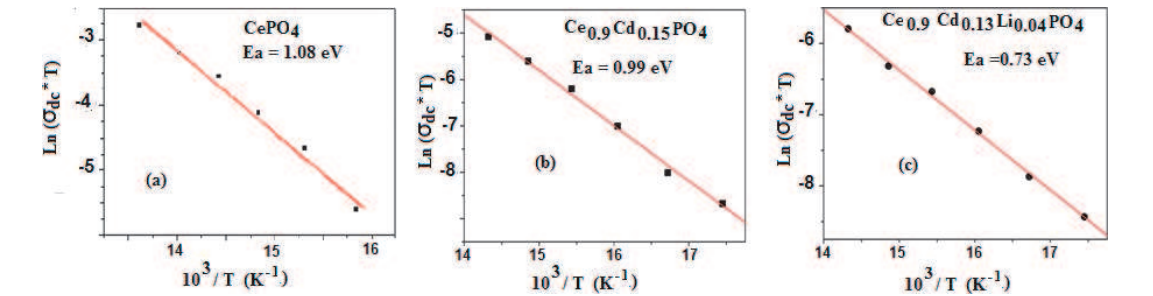
Figure 3.
Arrhenius plot of the electrical conductivity of CePO$_4$, Ce$_{0.9}$Cd$_{0.15}$PO$_4$ and Ce$_{0.9}$Cd$_{013}$Li$_{0.04}$PO$_4$.

$Cr_xCe_{1-x}PO_4$ Ea (eV) [40]	$Bi_xCe_{1-x}PO_4$ Ea (eV) [41]	$Ce_{0.9}Cd_{0.15-x}Li_{2x}PO_4$ Ea (eV) [42]
$CePO_4$ Ea = 1.08	$CePO_4$ Ea = 0.84	$CePO_4$ Ea = 1.08
$Cr_{0.08}Ce_{0.92}PO_4$ Ea = 0.90	$Bi_{0.02}Ce_{0.98}PO_4$ Ea = 0.87	$Ce_{0.9}Cd_{0.15}PO_4$ Ea = 0.99
$Cr_{0.10}Ce_{0.90}PO_4$ Ea = 0.84	$Bi_{0.08}Ce_{0.92}PO_4$ Ea = 1.09	$Ce_{0.9}Cd_{0.13}Li_{0.04}PO_4$ Ea = 0.72
$Cr_{0.20}Ce_{0.80}PO_4$ Ea = 0.80		

Table 2.
Activation energy of $Cr_xCe_{1-x}PO_4$, $Bi_xCe_{1-x}PO_4$ and $Ce_{0.9}Cd_{0.15-x}Li_{2x}PO_4$.

(A = area of the sample surface and t = sample thickness). The temperature dependence of dc-conductivity could be plotted based on the Arrhenius law with the following expression:

$$\sigma_{dc} = \frac{A_0}{T} \, e^{-\frac{Edc}{K.T}} \qquad (4)$$

where A_0 is the pre-exponential factor, Ea the activation energy and K the Boltzmann constant.

The activation energy of the undoped $CePO_4$ nanorods (Ea = 1.08 eV) is comparable to that obtained for $CePO_4$ nanosheets (Ea = 1.06 eV) [44]. It seems that the change of the morphology and the synthesis route used weakly affect the activation energy of the cerium phosphates. The activation energy deduced from Log (σT) as a function of 10^3/T (**Figure 3**) are summarized in **Table 2**.

The effect of Cr^{3+}, (Cd^{2+}, Li^+) substitutions decreases the activation energies with the increase in Cr, (Cd, Li)-concentration (**Table 2**). Consequently, the dc-conductivity of the as-prepared samples increases with temperature and with doping concentration. Lattice defects and distortions in the phosphate structure produced by the substitution allow the increase of the DC conductivity. The enhancement of activation energy could be related to the mobility of oxygen ions (O_2^-). This phenomenon has been observed by Nandini et al. [45]. They show that with an appropriate ratio of magnesium and strontium, the ionic conductivity increases as compared to that exhibited by ceria singly doped with Mg.

The difference in the electrical transport process between the Cr, Cd, Li doped $CePO_4$ and the Bi-doped $CePO_4$ results from the difference in atomic weight of Bi and Cr, Cd, Li. The atomic weight affects the mobility of the ions and therefore the Bi^{3+} ions remain close to their initial positions.

5. Electrochemical measurements

In order to explore the potential application of nonmaterials as cathode materials, their electrochemical performance with respect to Li insertion/extraction was investigated. Cyclic voltammograms (CVs) for $CePO_4$, $Ce_{0.9}Cd_{0.15}PO_4$ and $Bi_{0.02}Ce_{0.98}PO_4$ nanorods (examples) at 20 mV/s are shown in **Figure 1**. For all the as-prepared compounds, the cyclic voltammograms are well superposed indicating the relative structural stability under these conditions. The same shape of the CV curves slightly is observed for Nanoplate-like CuO in the presence of $LiClO_4$ in propylene carbonate [46].
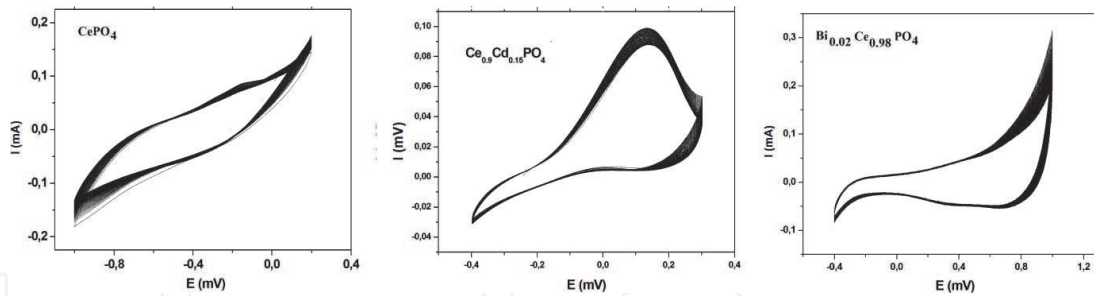
$CePO_4$, $Cd_{0.15}Ce_{0.90}PO_4$ and $Bi_{0.02}Ce_{0.98}PO_4$ based electrode cyclic voltammogramm.

These voltammograms indicate the intercalation/de-intercalation process of Li^+ ions. During the electrochemical redox processes, the intercalation/de-intercalation process of Li^+ ions can be represented by the following reaction:

$$M_xCe_{1-x}PO_4 + ye^- + yLi^+ \leftrightarrow Liy\, M_xCe_{1-x}PO_4$$

$$\text{Intercalation of Li} \rightarrow$$

$$\leftarrow \text{De} - \text{intercalation of Li}$$

The lithium ion diffusion coefficients can be calculated from the Randles-Sevcik law [47]:

$$ip = (2.69 \times 10^5)\, n^{(3/2)}.\, A\, C\, D_{Li}^{1/2}\, v^{1/2} \tag{5}$$

where ip is the peak current (A), n is the number of electrons exchanged, A is the apparent surface area of the electrode (cm^2), D_{li} and C are the diffusion coefficient (cm^2/s) and the analyte concentration (in moles/cm^3) respectively, and V is the potential scan rate (V/s). The lithium ion diffusion coefficients deduced are 2.5×10^{-9}, 0.7×10^{-9}, 4.6×10^{-9} $cm^2 s^{-1}$ for $CePO_4$, $Ce_{0.9}Cd_{0.15}PO_4$ and $Ce_{0.9}Cd_{0.13}Li_{0.04}PO_4$, respectively. The structure, surface area, grain size and morphology affect the calculated lithium diffusion coefficient DLi of the electrode materials. For example, Bi doping with the appropriate amount improved the electrochemical performance of $LiFePO_4$ cathode material, synthesized by the sol–gel method [48].

For as-prepared $Bi_xCe_{1-x}PO_4$ (x = 0.00, 0.02, 0.08) electrodes, The lithium ion diffusion coefficient (D_{Li}) values could be determined by using Nyquist plot through the relation [49]:

$$D_{Li} = \frac{R^2\, T^2\, V_M^2}{2A^2\, n^4\, F^4\, \sigma^2} \tag{6}$$

Where: F, R and T indicate Faraday constant, gas constant and room temperature, respectively.

(1). D_{Li} can be calculated as the Warburg impedance Z_w is inversely proportional to the square root of the diffusion coefficient as shown in [50]. The calculated lithium diffusion coefficient of the $CePO_4$ and $Bi_{0.02}Ce_{0.98}PO_4$ and $Bi_{0.08}Ce_{0.92}PO_4$ electrodes is 3.3×10^{-16}, 40×10^{-16} and 12.8×10^{-16} $cm^2.s^{-1}$ respectively. The D_{Li} variation values n can be attributed to creating the defect and increasing disorder of the lattice in doped $CePO_4$, drives to the improvement of the electrochemical performance. The structure of H-$CePO_4$-type characterized by infinite tunnels

Specific capacitances C (Fg⁻¹) [41]	Specific capacitances C (Fg⁻¹) [42]
CePO₄ C = 58	CePO₄ C = 58
Bi₀.₀₂Ce₀.₉₈PO₄ C = 63	Ce₀.₉Cd₀.₁₅PO₄ C = 76
Bi₀.₀₈Ce₀.₉₂PO₄ C = 75	Ce₀.₉Cd₀.₁₃Li₀.₀₄PO₄ C = 120

Table 3.
Specific capacitances of $Bi_xCe_{1-x}PO_4$ and $Ce_{0.9}Cd_{0.15-x}Li_{2x}PO_4$ nanomaterials.

provides fast ionic transport. The Li + ions can move quickly in an appropriate direction [51].

The specific capacitance can be estimated by the following equation [52, 53]:

$$C = \frac{\int I dv}{s.w.\Delta V} \tag{7}$$

where ΔV is the potential window, m is the mass of active material in one electrode, I is the current, and s is the potential scan rate. The variation of the specific capacitance of two prepared simples versus cycle number is given in **Table 3.** We show that the partial substitution of Ce by Cd increase the capacitance. The increasing of the capacitance can be attributed to the partial substitution and the small crystal size which improves the kinetics of electrochemical reactions and the structure which provides fast ionic transport.

The reason for the improvement of the discharge capacity can be explained as follows: with Bi-doping, the grain size of the particles decreases, which leads to the migration of the Li-ion.

The penetration of electrolyte ions and the electrochemical activation of the materials may increase the specific capacitance. A similar phenomenon has been observed by other authors [54, 55].

Doped samples show better performance in terms of discharge capacity than undoped ones. These results could be attributed to the contribution of the nanorod shape and the particle size. Indeed, the reduction of the size allows a faradic reaction providing a short ion diffusion path and electron transport.

6. Conclusion

In summary, we have demonstrated a rapid and convenient hydrothermal method for the preparation of doped and undoped CePO₄ nanomaterials. The Cr³⁺, Bi³⁺, Cd²⁺ and Li⁺ ions substitution affects the optical, electrical and electrochemical properties. The band gap energies of the as-prepared CePO₄ nanorods decreased with increasing doping-concentration showing a red-shift trend. Comparative experiments have witnessed that the doped-CePO₄ electrode had the most excellent electrochemical properties in comparison with undoped CePO₄ nanomaterials. The electrochemical results show that the specific capacity and the electrical conductivity increase with increasing doping content. The specific capacitance of the hybrid electrode materials presents a good cyclic stability. The improved specific capacitance is due to the surface morphology and the decrease of grain size of the particles. The lowering in the crystal size allows a fast faradaic reaction, giving a short ion diffusion path, which improves the electrochemical properties. This simple synthesis methodology together with the good optical and electronic properties makes this material scientifically; technologically interesting and could find a potential use in nanoelectronics.

Author details

Salah Kouass[1*], Amor Fadhalaoui[2], Hassouna Dhaouadi[3] and Fathi Touati[3]

1 Laboratoire Matériaux Utiles, Institut National de Recherche et d'Analyse Physico-chimique (INRAP), Sidi Thabet, Tunis, Tunisie

2 Laboratoire de Physique des Matériaux, Faculté des Sciences de Bizerte, Université de Carthage, Zarzouna, Bizerte, Tunisia

3 Laboratoire Matériaux Traitement et Analyse, Institut National de Recherche et d'Analyse Physico-chimique (INRAP), Sidi Thabet, Tunis, Tunisie

*Address all correspondence to: koissa2000@yahoo.fr

IntechOpen

References

[1] Asiya SI, Kaushik P, Gharieb El-S, Abd Elkodous M, Demetriades C, Kralj S, et al. Reliable optoelectronic switchable device implementation by CdS nanowires conjugated bent-core liquid crystal matrix. Organic Electronics. 2020;**82**:10559

[2] Ho LN, Nishiguchi H, Nagaoka K, Takita Y. Synthesis and characterization of a series of mesoporous nanocrystalline lanthanides phosphate. Journal of Porous Materials. 2006;**13**: 237-244

[3] Zhang YJ, Guan HM. The growth of lanthanum phosphate (rhabdophane) nanofibers via the hydrothermal method. Materials Research Bulletin. 2005;**40**:1536-1543

[4] Hikichi Y, Nomura T, Tanimura Y, Sb S. Sintering and properties of monazite-type $CePO_4$. Journal of the American Ceramic Society. 1990;**73**: 3594-3596

[5] Xu L, Guo G, Uy D, O'Neill AE, Weber WH, Rokosz MJ, et al. Cerium phosphate in automotive exhaust catalyst poisoning. Applied Catalysis B: Environmental. 2004;**50**:113-125

[6] Granados ML, Galisteo FC, Lambrou PS, Mariscal R, Sanz J, Sobrados I, et al. Role of P-containing species in phosphated CeO_2 in the deterioration of its oxygen storage and release properties. Journal of Catalysis. 2006;**239**:410-421

[7] Di W, Wang X, Ren X. Nanocrystalline $CePO_4$:Tb as a novel oxygen sensing material on the basis of its redox responsive reversible luminescence. Nanotechnology. 2010; **21**:075709

[8] Kitamura N, Amezawa K, Tomii Y, Hanada T, Yamamoto N, Omata T, et al. Electrical conduction properties of Sr-doped $LaPO_4$ and $CePO_4$ under oxidizing and reducing conditions. Journal of the Electrochemical Society. 2005;**152**:A 658-A 663

[9] Feng X, Cheng Y, Ye C, Ye J, Peng J, Hu J. Synthesis and Ag-content-depended electrochemical properties of Ag/ZnO heterostructured nanomaterials. Materials Letters. 2012; **79**:205-208

[10] Hu J, Yu Y, Guo H, Chen Z, Li A, Feng X, et al. Sol–gel hydrothermal synthesis and enhanced biosensing properties of nanoplated lanthanum-substituted bismuth titanate microspheres. Journal of Materials Chemistry. 2011;**21**:5352-5359

[11] Yang M, You H, Liu K, Zheng Y, Guo N, Zhang H. Low-temperature coprecipitation synthesis and luminescent properties of $LaPO_4$:Ln^{3+} (Ln^{3+} = Ce^{3+}, Tb^{3+}) nanowires and $LaPO_4$:Ce^{3+},Tb^{3+}/$LaPO_4$ core/shell nanowires. Inorganic Chemistry. 2010; **49**:4996-5002

[12] del Moral EG, Fagg DP, Chinarro E, Abrantes JCC, Jurado JR, Mather GC. Impedance analysis of Sr-substituted $CePO_4$ with mixed protonic and p-type electronic conduction. Ceramics International. 2009;**35**:1481-1486

[13] Norby T, Christiansen N. Proton conduction in Ca- and Sr-substituted $LaPO_4$. Solid State Ionics. 1995;**77**:240-243

[14] Ding X, Liu Y, Gao L, Guo L. Effects of cation substitution on thermal expansion and electrical properties of lanthanum chromites. Journal of Alloys and Compounds. 2006;**425**:318-322

[15] Yunus SM, Yamauchi H, Zakaria H, Igawa N, Hoshikawa A, Ishii Y. Neutron diffraction studies of the magnetic ordering in the spinel oxide system

$Mg_xCo_{1-x}Cr_xFe_{2-x}O_4$. Journal of Alloys and Compounds. 2008;**455**:98-105

[16] Wahba AM, Mohamed MB. Structural, magnetic, and dielectric properties of nanocrystalline Cr-substituted $Co_{0.8}Ni_{0.2}Fe_2O_4$ ferrite. Ceramics International. 2014;**40**: 6127-6135

[17] Li G, Zhang D, Yu JC, Leung MKH. An efficient bismuth tungstate visible-light-driven photocatalyst for breaking down nitric oxide. Environmental Science & Technology. 2010;**44**: 4276-4281

[18] Bessekhouad Y, Mohammedi M, Trari M. Hydrogen photoproduction from hydrogen sulfide on Bi_2S_3 catalyst. Solar Energy Materials & Solar Cells. 2002;**73**:339-350

[19] ShimodairaY KH, Kobayashi H, Kudo A. Photophysical properties and photocatalytic activities of bismuth molybdates under visible light irradiation. The Journal of Physical Chemistry. B. 2006;**110**:17790-17797

[20] Xiong J, Cheng G, Lu Z, Tang J, Yu X, Chen R. BiOCOOH hierarchical nanostructures: Shape-controlled solvothermal synthesis and photocatalytic degradation performances. CrystEngComm. 2011;**13**: 2381-2390

[21] Tang J, Zou Z, Ye J. Efficient photocatalytic decomposition of organic contaminants over $CaBi_2O_4$ under visible-light irradiation. Angewandte Chemie, International Edition. 2004;**43**: 4463-4466

[22] Kang F, Zhang Y, Peng M. Controlling the energy transfer via multi luminescent centers to achieve white light/tunable emissions in a single-phased X2-Type Y_2SiO_5:Eu^{3+}, Bi^{3+} phosphor for ultraviolet converted LEDs. Inorganic Chemistry. DOI: 10.1021/ic502439k

[23] Kang F, Peng M, Zhang Q, Qiu J. Abnormal anti-quenching and controllable multi-transitions of Bi^{3+} luminescence by temperature in a yellow-emitting $LuVO_4$:Bi^{3+} phosphor for UV-converted white LEDs. Chemistry - A European Journal. 2014; **20**:11522-11530

[24] Arabzadeh A, Salimi A. One dimensional CdS nanowire@TiO_2 nanoparticles core-shell as high performance photocatalyst for fast degradation of dye pollutants under visible and sunlight irradiation. Journal of Colloid and Interface Science. 2016; **479**:43

[25] Lee SM, Yeon DH, Chon SS, Cho YS. Effect of double substitutions of Cd and Cu on optical band gap and electrical properties of non-colloidal PbS thin films. Journal of Alloys and Compounds. 2016;**685**:129

[26] Xiao Y, Chun F, Zhang J, Han I. Electrical structures, magnetic polaron and lithium ion dynamics in three transition metal doped $LiFe_{1-x}M_xPO_4$ (M = Mn, Co and La) cathode material for Li ion batteries from density functional theory study. Solid State Ionics. 2016;**294**:73-81

[27] Yuan H, Wang X, Wu Q, Shu H, Yang X. Effects of Ni and Mn doping on physicochemical and electrochemical performances of $LiFePO_4$/C. Journal of Alloys and Compounds. 2016;**675**:187-194

[28] Zhou H, Upreti S, Chernova NA, Hautier G, Ceder G, Whittingham MS. Iron and manganese pyrophosphates as cathodes for lithium-ion batteries. Chemistry of Materials. 2011;**23**:293

[29] Thirugnanasambandan T, Pal K, Sidhu A, Elkodous MA, Prasath H, Kulasekarapandian K, et al. Aggrandize efficiency of ultra-thin silicon solar cell via topical clustering of silver nanoparticles. Nano-Structures & Nano-Objects. 2018;**16**:224-233

[30] Cao M, Hu C, Wu Q, Guo C, Qi Y, Wang E. Controlled synthesis of LaPO₄ and CePO₄ nanorods/nanowires. Nanotechnology. 2005;**16**:282-286

[31] Pala K, Maitia UN, Majumdera TP, Debnath SC. A facile strategy for the fabrication of uniform CdS nanowires with high yield and its controlled morphological growth with the assistance of PEG in hydrothermal route. Applied Surface Science. 2011; **258**:163-168

[32] Bao J, Yu R, Zhang J, Yang X, Wang D, Deng J, et al. Low-temperature hydrothermal synthesis and structure control of nano-sized CePO₄. CrystEngComm. 2009;**11**:1630

[33] Ma L, Chen W-X, Zheng Y-F, Xu Z-D. Hydrothermal growth and morphology evolution of CePO₄ aggregates by a complexing method. Materials Research Bulletin. 2008;**43**: 2840

[34] Yan RX, Sun XM, Wang X, Peng Q, Li YD. Crystal structures, anisotropic growth, and optical properties: Controlled synthesis of lanthanide orthophosphate one-dimensional nanomaterials. Chemistry - A European Journal. 2005;**11**:2183

[35] Zollfrank C, Scheel H, Brungs S, Greil PJ. Europium(III) orthophosphates: Synthesis, characterization, and optical properties. Crystal Growth & Design. 2008;**8**:766

[36] Guo D, Hu C, Xi Y. Synthesis and magnetic property of Fe doped LaPO₄ nanorods. Applied Surface Science. 2013;**268**:458-463

[37] Wu L, Wang Z, Li X, et al. Electrochemical performance of Ti⁴⁺-doped LiFePO₄ synthesized by co-precipitation and post-sintering method. Transactions of the Nonferrous Metals Society of China. 2010;**20**: 814-818

[38] Miyake Y, Tada H. Photocatalytic degradation of methylene blue with metal doped mesoporous titania under irradiation of white light. Journal of Chemical Engineering of Japan. 2004; **37**:630-635

[39] Tauc J, Menth A. States in the gap. Journal of Non-Crystalline Solids. 1972; **8–10**:569-585

[40] Fadhalaouia A, Dhaouadib H, Marouania H, Koukic A, Madanid A, Rzaiguia M. Cr-substitution effect on structural, optical and electrical properties of Cr$_x$Ce$_{1-x}$PO₄ (x = 0.00, 0.08; 0.10 and 0.20) nanorods. Materials Research Bulletin. 2016;**73**:153-163

[41] Fadhalaoui A, Kouass S, Dhaouadi H. Bi$_x$Ce$_{1-x}$PO₄ (x = 0.00, 0.02, and 0.08) nanorods: Structural, electrical, optical, and electrochemical properties. Ionics. 2018;**24**:429-450

[42] Kouass S, Fadhalaoui A, Dhaouadi H, Touati F. Electrical and electrochemical properties of undoped CePO₄ and doped Ce$_{0.9}$Cd$_{0.15-x}$Li$_{2x}$PO₄ nanomaterials (x = 0 and 0.02). Materials Letters. 2018;**217**:75-78

[43] Correcher V, Isasi J, Cubero A, Pérez M, Aldama I, Arévalo P, et al. Structural and luminescence characterization of synthetic Cr-doped Ni₃(PO₄)₂. Journal of Physics and Chemistry of Solids. 2013;**74**: 1678-1682

[44] Dhaouadi H, Fadhalaoui A, Mdani A, Rzaigui M. Structural and electrical properties of nanostructured cerium phosphate. Ionics. 2014;**20**: 857-866

[45] Jaiswal N, Kumar D, Upadhyay S, Parkash O. Effect of Mg and Sr co-doping on the electrical properties of ceria-based electrolyte materials for intermediate temperature solid oxide fuel cells. Journal of Alloys and Compounds. 2013;**577**:456-462

[46] Janene F, Dhaouadi H, Arfaoui L, Etteye N, Touati F. Nanoplate-like CuO: Hydrothermal synthesis, optical and electrochemical properties. Ionics. 2015;**21**:477-485

[47] Tian L, Zhong X, Hu W, Liu B, Li Y. Fabrication of cubic PtCu nanocages and their enhanced electrocatalytic activity towards hydrogen peroxide. Nanoscale Research Letters. 2014;**9**: 68-73

[48] Fuwei M, Dongchen W, Zhufa Z, Shumei W. Structural and electrochemical properties of LiFe$_{1-3x/2}$Bi$_x$PO$_4$/C synthesized by sol-gel. Ionics. 2014;**20**:1665-1669

[49] Wang L, Ma P, Zhang Y, Gao C, Yan C. Determination of Li-ion diffusion coefficient *via* Coulometric titration and electrochemical impendence method. Journal of Salt Lake Research. 2009;**17**:52-55

[50] Franger S, Cras FL, Bourbon C, Rouault H. LiFePO$_4$ synthesis routes for enhanced electrochemical performance. Electrochemical and Solid-State Letters. 2002;**5**(10):A231-A233

[51] Mengyu Y, Guobin Z, Qiulong W, Xiaocong T, Kangning Z, Qinyou A, et al. In operando observation of temperature-dependent phase evolution in lithium-incorporation olivine cathode. Nano Energy. 2016;**22**:406-413

[52] Conway BE. Transition from "supercapacitor" to "battery" behavior in electrochemical energy storage. Journal of the Electrochemical Society. 1991;**138**:1539-1548

[53] Kuo SL, Wu NL. Electrochemical capacitor of MnFe$_2$O$_4$ with organic Li-ion electrolyte. Electrochemical and Solid-State Letters. 2007;**10**:A171-A175

[54] Huang T, Zhao C, Qiu Z, Luo J, Hu Z. Hierarchical porous ZnMn$_2$O$_4$ synthesized by the sucrose-assisted combustion method for high-rate supercapacitors. Ionics. 2017;**23**:139-146

[55] Xuefei D, Hailei Z, Yao L, Zijia Z, Andrzej K, Konrad Ś. Synthesis of core-shell-like ZnS/C nanocomposite as improved anode material for lithium ion batteries. Electrochimica Acta. 2017;**228**: 100-106